ACS APPLIED MATERIALS & INTERFACES

www.acsami.org

Research Article

Energy Harvesting Floor from Commercial Cellulosic Materials for a Self-Powered Wireless Transmission Sensor System

Long Gu,[§] Lazarus German,[§] Tong Li, Jun Li, Yan Shao, Yin Long, Jingyu Wang, and Xudong Wang*

Cite This: *ACS Appl. Mater. Interfaces* 2021, 13, 5133–5141

Read Online

ACCESS | Metrics & More | Article Recommendations | Supporting Information

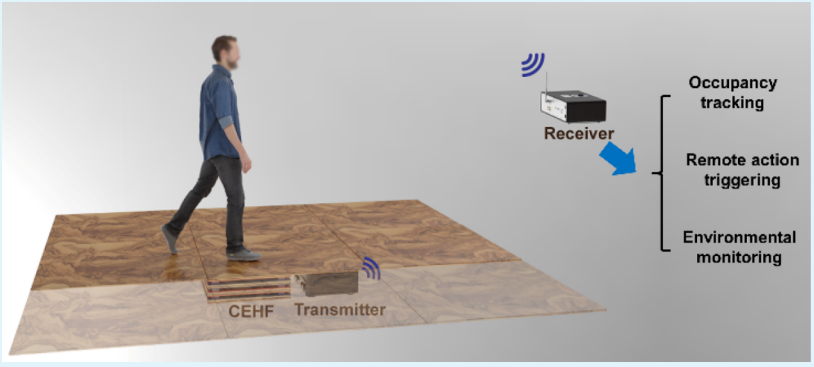

ABSTRACT: Cellulose-based materials have gained increasing attention for the development of low-cost, eco-friendly technologies, and more recently, as functional materials in triboelectric nanogenerators (TENGs). However, the low output performance of cellulose-based TENGs severely restricts their versatility and employment in emerging smart building and smart city applications. Here, we report a high output performance of a commercial cellulosic material-based energy harvesting floor (CEHF). Benefiting from the significant difference in the triboelectric properties between weighing and nitrocellulose papers, high surface roughness achieved by a newly developed mechanical exfoliation method, and large overall contact area via a multilayered device structure, the CEHF (25 cm × 15 cm × 1.2 cm) exhibits excellent output performance with a maximum output voltage, current, and power peak values of 360 V, 250 μA, and 5 mW, respectively. It can be directly installed or integrated with regular flooring products to effectively convert human body movements into electricity and shows good durability and stability. Moreover, a wireless transmission sensing system that can produce a 1:1 footstep-to-signal (transmitted and received) ratio is instantaneously powered by a TENG based entirely on cellulosic materials for the first time. This work provides a feasible and effective way to utilize commercial cellulosic materials to construct self-powered wireless transmission systems for real-time sensing applications.

KEYWORDS: *triboelectric nanogenerator, cellulose materials, energy harvesting floor, self-powered sensor, paper products*

INTRODUCTION

With the rapid development of Internet of Things (IoT) technology, a huge number of intelligent electronic devices such as smart portable/wearable electronic devices, biomedical implantable electronic devices, and sensor networks have been widely applied in all spheres of human life.[1−5] Such IoT networks can give us valuable insights on human interactions—whether between each other or with their environment—and the functions and performance of interconnected systems that might otherwise be overlooked. For instance, information from occupancy sensors enables us to make agile and, at times, remote decisions for optimizing flooring layouts (e.g. retail space, trade show booths, and high performance workspaces) or the functions of automated systems (e.g. HVAC and lighting and safety alerts in security or healthcare). However, the increased employment of these electronic devices is greatly challenged by the increasing demand for sustainable, consolidated power supplies that avoid periodic power checks or replacement of batteries, alleviate space limitations, and eliminate wiring costs.[6] To address these problems, many energy harvesting technologies based on the piezoelectric effect,[7−9] electromagnetic induction,[10] pyroelectric effect,[11,12] and triboelectric effect[13−15] have been exploited to convert ambient environmental energy into useful electrical power so that electronic devices can be self-powered. Among these technologies, a triboelectric nanogenerator (TENG), which benefits from low-cost, abundant and flexible

Received: November 19, 2020
Accepted: January 11, 2021
Published: January 20, 2021

https://dx.doi.org/10.1021/acsami.0c20703
ACS Appl. Mater. Interfaces 2021, 13, 5133−5141

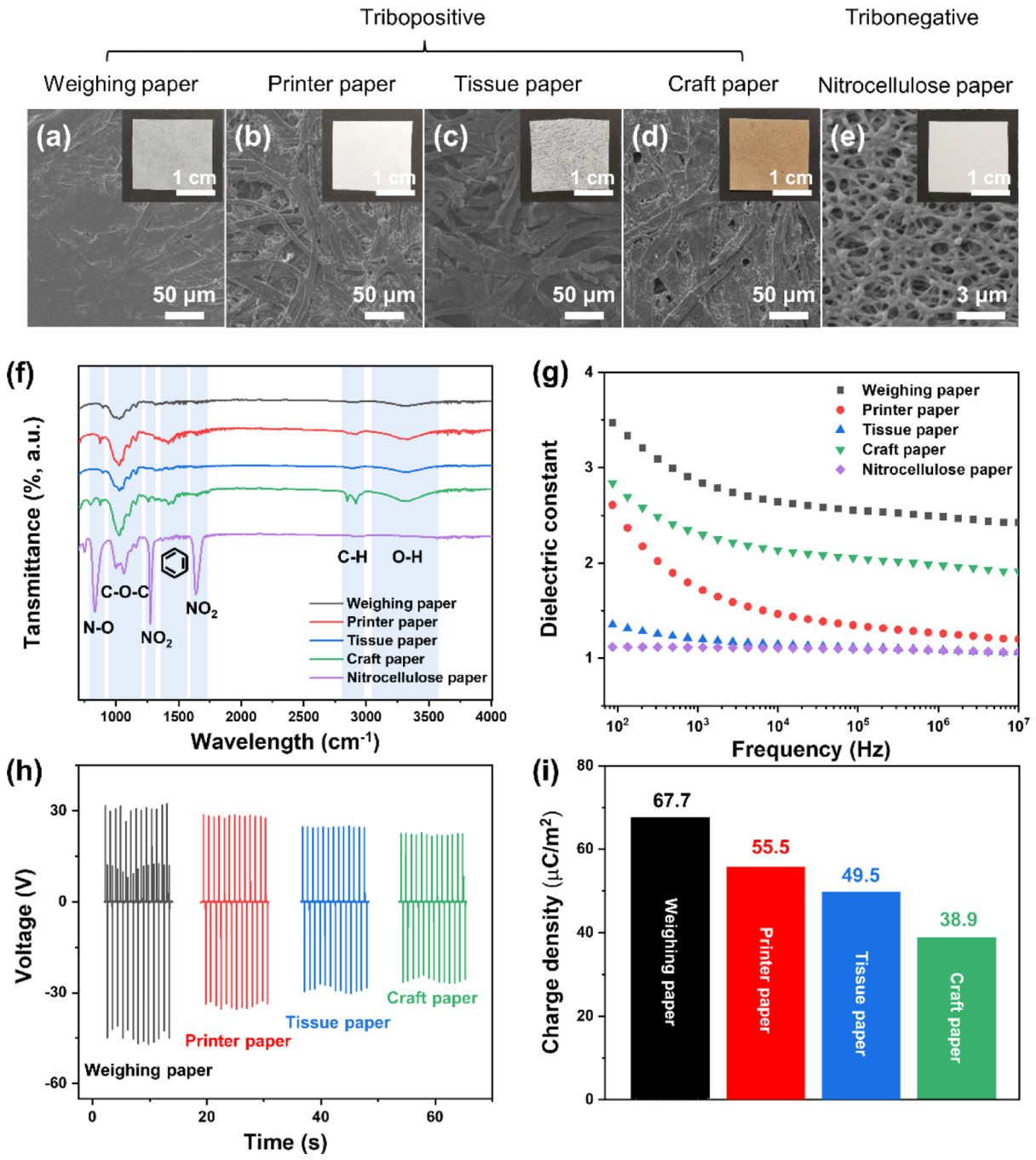

Figure 1. Characterization of different paper products. (a–d) SEM images of weighing paper, printer paper, tissue paper, and craft paper which act as tribopositive materials. (e) SEM image of nitrocellulose paper which acts as the tribonegative material. Insets are optical images of these paper products. (f) FTIR spectra and (g) frequency dependence of the dielectric constant of these paper products. (h) Output voltage of the four tribopositive paper products vs nitrocellulose paper and (i) the corresponding charge density of different combinations.

materials, easy and scalable fabrication, high energy conversion efficiency, and high cycle fatigue characteristics, shows great potential to be a power source in realizing self-powered systems.

To achieve high output power, more conventional triboelectric materials (e.g. tribopositive Al, Cu, nylon and tribonegative polyimide, polyvinylidene fluoride, fluorinated ethylene propylene, and polytetrafluoroethylene)[16−20] and surface roughening techniques (e.g. plasma processing, etching, freeze-drying, and electrospinning)[21−25] are the preferred choice. However, these materials are relatively expensive, nonrenewable and have environmentally unfriendly end-of-life. Moreover, the aforementioned roughening techniques require expensive equipment and complicated processes. Alternatively, cellulosic materials (wood pulp, cotton, paper, and hemp) comprise the most abundant natural polymer source in the world and have increasingly gained attention as a renewable, biodegradable, and cost-effective option for high-performance TENGs.[26−31] For instance, Yao et al.[27] built TENGs that used cellulose derivatives as the tribonegative and tribopositive materials realized through chemical functionalization. The enhanced electron loss/gain of nitrated/methylated cellulose

https://dx.doi.org/10.1021/acsami.0c20703
ACS Appl. Mater. Interfaces 2021, 13, 5133−5141

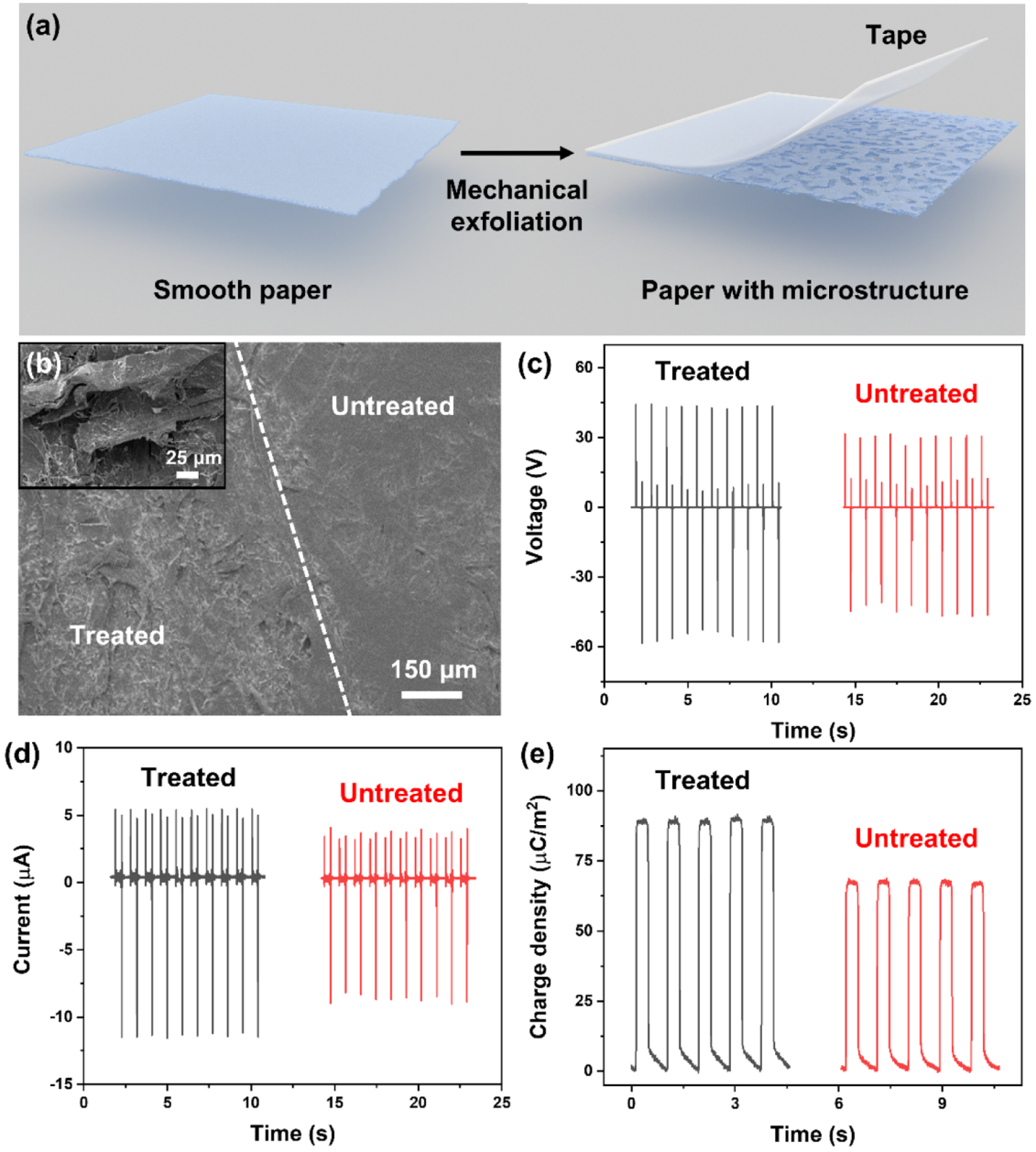

Figure 2. Influence of surface microstructures on the output of the TENG. (a) Schematic illustration of the mechanical exfoliation method for microstructure fabrication on paper. (b) SEM image of a partially treated weighing paper. Inset is an enlarged view of the treated side. (c) Output voltage, (d) current of treated and untreated weighing paper paired with nitrocellulose paper, and (e) their corresponding charge density vs nitrocellulose paper.

derivatives provided an effective pathway to develop fully cellulose-based TENGs. Subsequently, attracted by a mature production technology, low cost and easy large-scale fabrication, Chen et al.[28] developed a TENG based on commercial cellulosic materials (printer paper paired with nitrocellulose membranes). Despite these advancements, cellulosic material-based TENGs have not yet achieved sufficient outputs to instantaneously power some higher energy devices such as wireless transmission systems. To do so, we may address other factors in TENG design such as contact area between the triboelectric materials (surface roughness) and multilayered architectures.

In order to real-time power a wireless transmission sensor system with a 1:1 footstep-to-signal (transmitted and received) ratio, here we developed a high performance, cellulosic material-based energy harvesting floor (CEHF) by utilizing commercially available weighing paper and nitrocellulose paper (different kinds of paper are used to represent commercial cellulosic materials in this work). Benefiting from the significant difference of triboelectric properties between weighing paper and nitrocellulose paper, surface roughening of weighing paper via a newly developed mechanical exfoliation method, and large effective contact area resulted by a multilayered device structure, our CEHF exhibited excellent output performance with a maximum output voltage, current, and power peak values of 360 V, 250 μA, and 5 mW, respectively. A self-powered wireless transmission sensor system was demonstrated to be able to produce and transmit a wireless signal upon each footstep, which showed a great

https://dx.doi.org/10.1021/acsami.0c20703
ACS Appl. Mater. Interfaces 2021, 13, 5133−5141

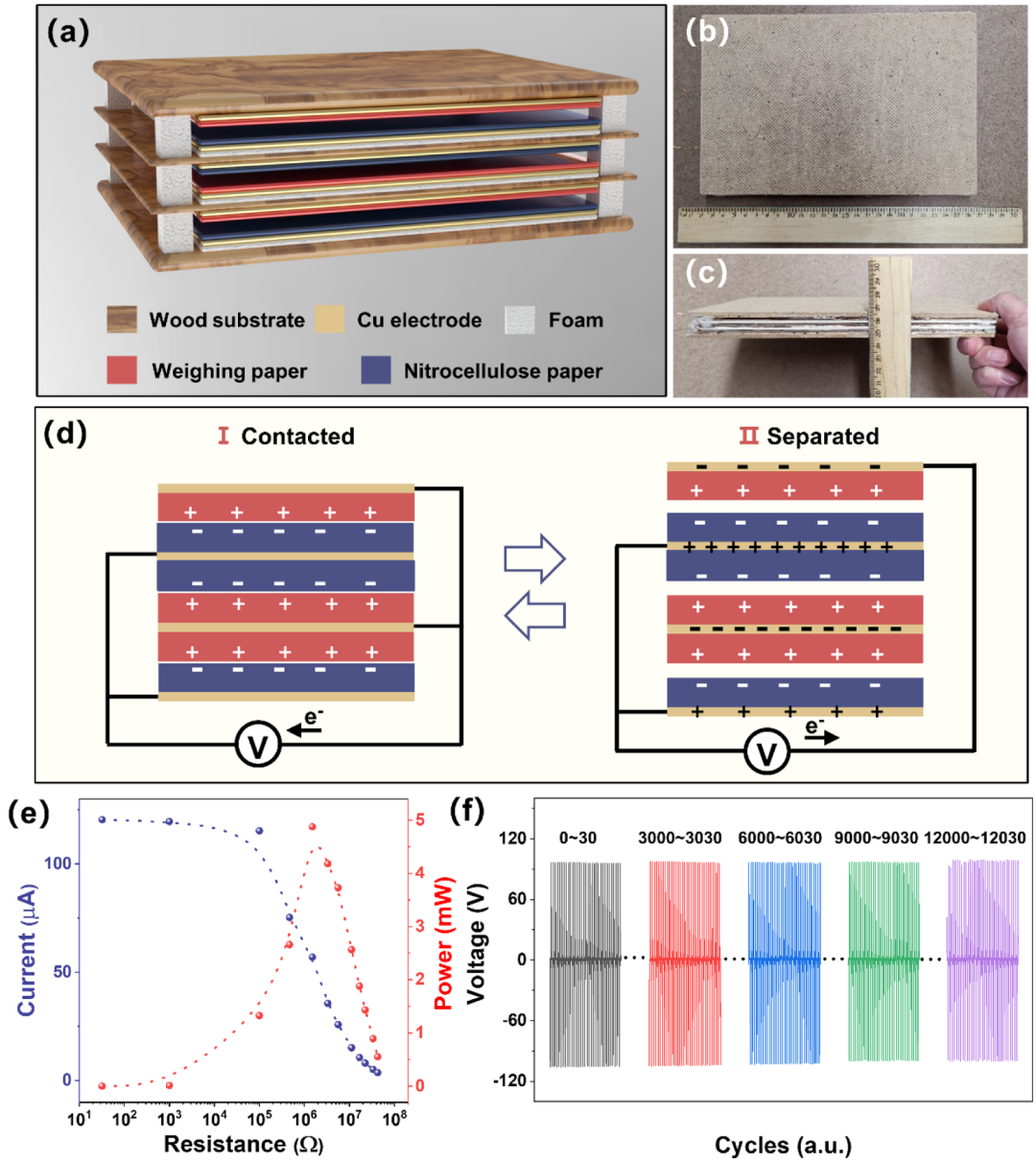

Figure 3. Design and characterization of the CEHF. (a) Illustration of the CEHF. (b) Top and (c) side views of the actual CEHF device. (d) Working principle of the multilayered CEHF. € Output current and power of CEHF vs external load resistance. (f) Output voltage of the CEHF as a function of working cycles.

potential in constructing self-powered wireless transmission systems for future smart buildings and cities.

RESULTS AND DISCUSSION

Since the capabilities of nitrocellulose paper have been repeatedly proven, it was used as the tribonegative material for all TENGs in this study. More conventional papers were hypothesized to be more tribopositive versus nitrocellulose since paper-making processes had limited functionalization pathways. To test this and explore viable options for a high performance tribopositive cellulosic material, we examined four representative commercial paper products: weighing paper, printer paper, tissue paper, and crafting paper. The surface structures of the tribopositive candidates and nitrocellulose paper were characterized using a scanning electron microscope (SEM) and are shown in Figure 1a–e. Insets are the corresponding optical images of these paper products. Among the four tribopositive papers, weighing paper showed the smoothest surface and highest compactness due to smaller cellulose fibers and repetitive calendaring technique in the fabrication process, and the tissue paper showed roughest surface and loosest structure. There were also some differences between the composition of the four papers. The Fourier transform infrared (FTIR) spectra in Figure 1f showed that all the four papers had characteristic peaks of cellulose around 1028, 2890, and 3325 cm^{-1}, which were associated with the C–O–C pyranose ring skeletal vibration, C–H stretching, and O–H stretching, respectively.[28] Craft paper also had the vibration peaks of the aromatic ring around 1400–1600 cm^{-1} which was generated by large amount of lignin.[32] For a TENG with contact-separation working mode, the triboelectric potential (V) between the two electrodes can be described as the following equation

https://dx.doi.org/10.1021/acsami.0c20703
ACS Appl. Mater. Interfaces 2021, 13, 5133–5141

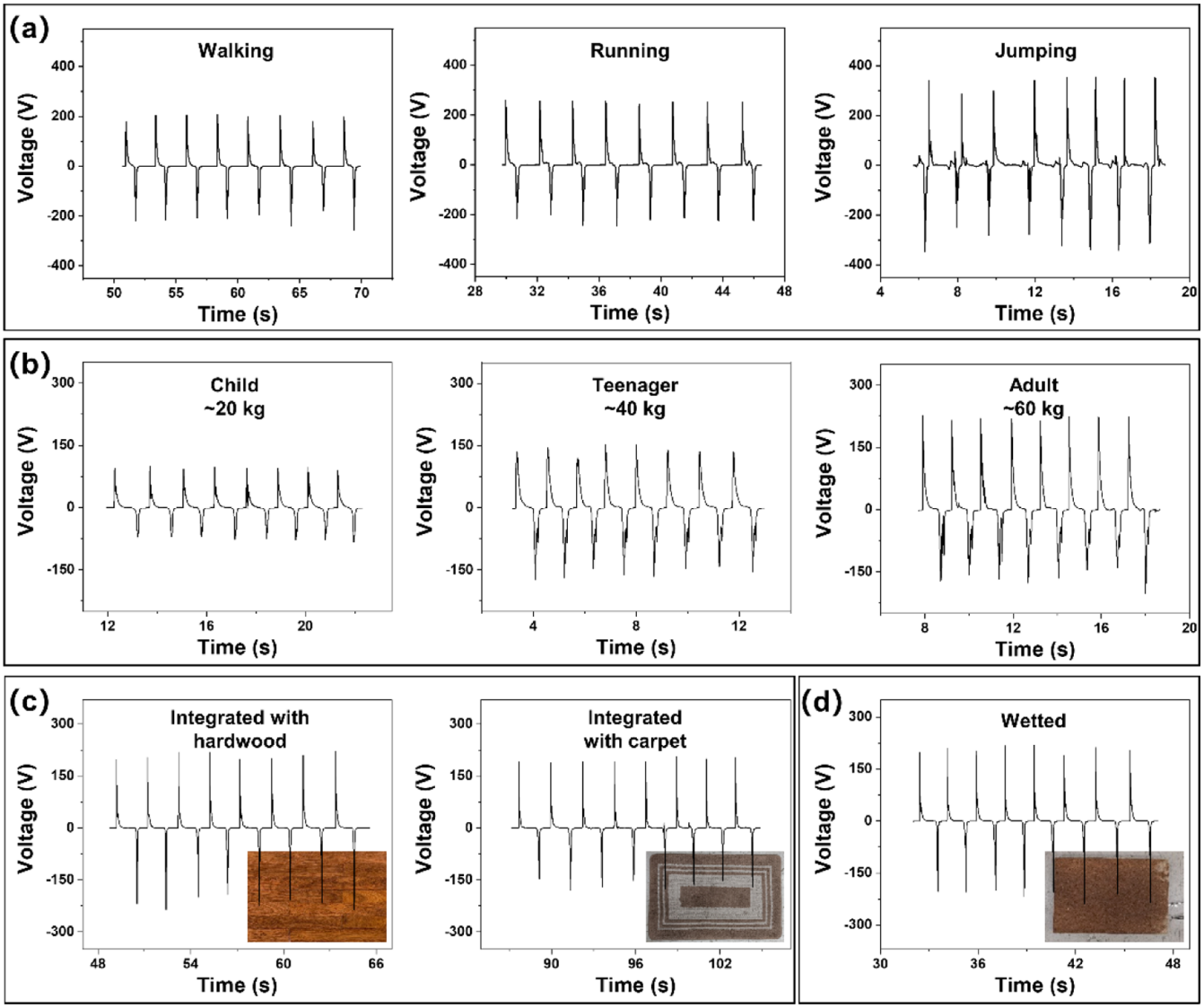

Figure 4. Output performance of the CEHF under different working conditions. (a) Output voltage of the CEHF driven by different motion forms of an adult (~60 kg). (b) Output voltage of the CEHF driven by people with different weights. (c) Output voltage of the CEHF integrated with hardwood and carpet flooring materials. (d) Output voltage of the CEHF wetted by water.

$$V = \frac{\sigma X(t)}{\varepsilon_0} - \frac{Q}{S\varepsilon_0}\left(\frac{d_1}{\varepsilon_1} + \frac{d_2}{\varepsilon_2} + X(t)\right)$$

where σ and Q are the surface charge density and the induced charge quantity on the electrode, respectively. d_i and ε_i represent the thickness and permittivity of the two friction materials, S is the electrode area, $X(t)$ is the gap distance between the surfaces of the two friction materials, and ε_0 is the vacuum permittivity.[33] Hence, besides surface roughness and composition, dielectric constant is another important factor for the output performance of the TENG. Figure 1g shows the frequency-dependent dielectric behavior of the four papers in the frequency range of 10^2 to 10^7 Hz. Determined by the compactness and composition of paper, the four papers' dielectric constant, from high to low, was weighing paper, craft paper, printer paper, and tissue paper. The FTIR spectrum and dielectric constant of nitrocellulose paper were also characterized and are shown in Figure 1f,g, respectively. NO_2 symmetric stretching around 1279 and 1650 cm^{-1} and N−O stretching around 839 cm^{-1} peaks in Figure 1f indicated that abundant nitro groups were present in the nitrocellulose paper. Its porous structure led to a rough surface and low dielectric constant which could be seen in Figure 1g.

According to the working mechanisms of TENGs, materials with greater electron loss/gain affinities, rougher surface, and higher dielectric constant are key factors for enhancing TENG output performance. However, none of the four aforementioned tribopositive papers have these attributes simultaneously. In order to check their actual triboelectric property, the four papers were used to pair with nitrocellulose paper, respectively, assembling four TENGs with commonly used contact-separation working mode. With an area of 2 × 2 cm^2 and separation distance of 1 cm, the output voltage and charge density of these TENGs were measured and are shown in Figure 1h,i. It could be found that the weighing and printer papers generated higher output voltage and charge density than tissue paper despite having smoother surfaces than tissue paper, which meant that the dielectric constant likely played a leading role here. Hence, weighing paper was the best choice

https://dx.doi.org/10.1021/acsami.0c20703
ACS Appl. Mater. Interfaces 2021, 13, 5133−5141

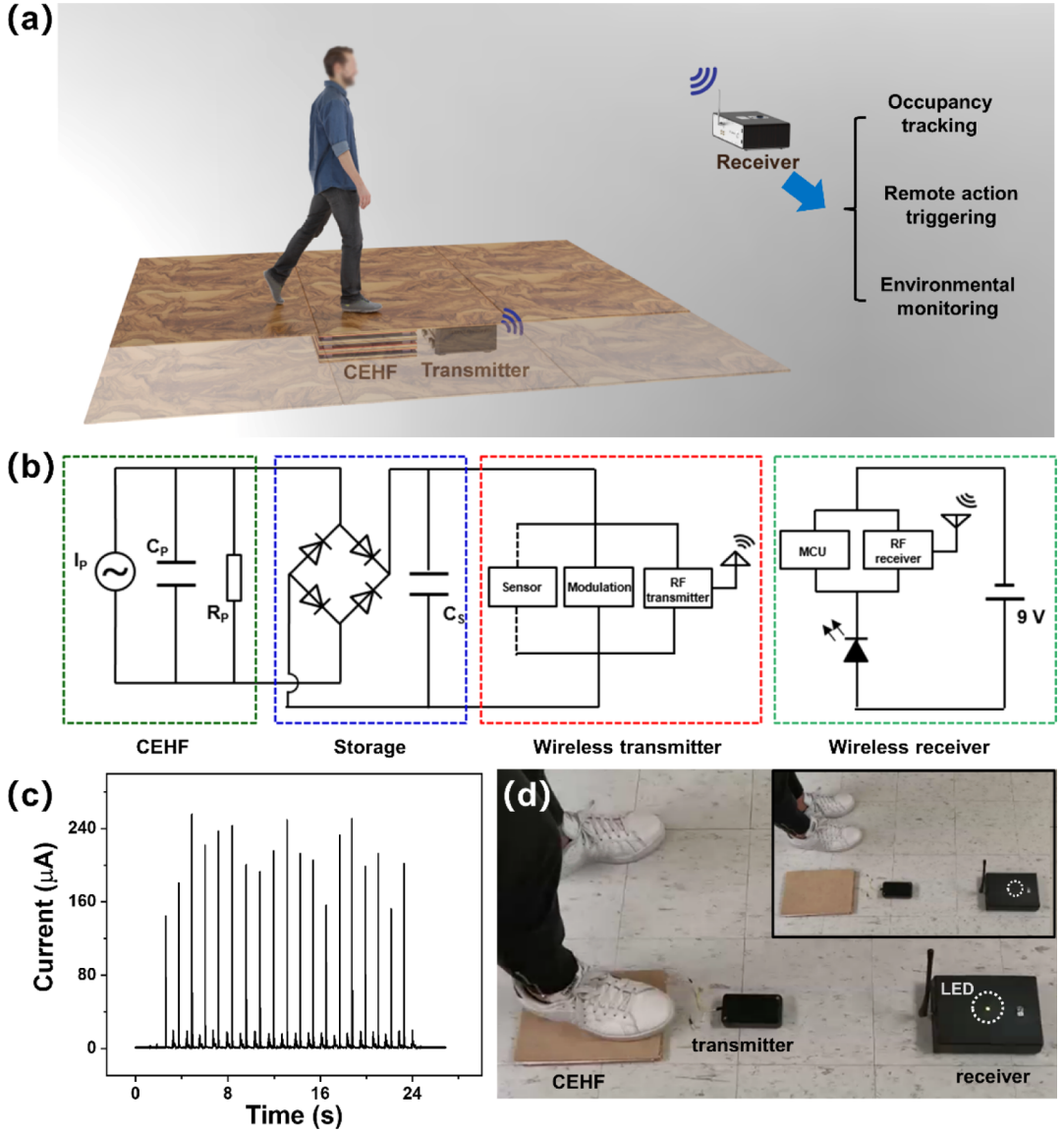

Figure 5. Application of the CEHF as a self-powered sensor. (a) Schematic illustration of a real-time wireless transmission sensing system for occupancy tracking, remote action triggering, environmental monitoring, etc. (b) Circuit diagram of the wireless transmission sensing system. (c) Rectified output current of the CEHF driven by human steps. (d) Instantaneous powering of a wireless transmission sensing system when people step on the CEHF.

for designing a high performance CEHF among these four candidates.

Because of its smooth surface, we may further enhance the triboelectric ability of the weighing paper through surface roughening. To address this issue, we developed a simple, cost-effective, and scalable fabrication method to introduce rough surface structures on the weighing paper. Figure 2a schematically shows this mechanical exfoliation method for surface microstructure fabrication. Commonly, a commercial scotch tape was tightly adhered to the surface of weighing paper and subsequently removed, resulting in non-uniform breakage of the surface fibers. To compare pre- and post-processed surfaces, weighing paper was partially treated by the mechanical exfoliation method with the surface morphology characterized by SEM and is shown in Figure 2b. In order to investigate the influence of this roughened surface structure on the output performance, the treated and untreated weighing papers were paired with nitrocellulose paper to assemble TENG devices. Each with areas of 2 × 2 cm^2 and separation distances of 1 cm, their output voltage, current, and charge density were measured and are shown in Figure 2c−e. By introducing a surface microstructure on the weighing paper, the peak values of output voltage, current, and charge density were increased from 45 V, 8.5 μA, and 67.7 $\mu C/m^2$ to 58 V, 11.5 μA, and 89.5 $\mu C/m^2$, respectively, which indicated that mechanical exfoliation method was an effective way to fabricate the microstructure on the paper's surface for enhancing the output performance of cellulosic material-based TENGs.

Next, we developed a high performance CEHF based on the treated weighing paper and nitrocellulose paper. Figure 3a shows a schematic model of our multilayered CEHF consisting of three units sandwiched between two wooden floor surfaces. Each unit was composed of a treated weighing paper/Cu layer, a spacer, and a nitrocellulose paper/Cu layer. Figure 3b,c shows the optical images of a real CEHF device with size of 25 cm × 15 cm × 1.2 cm, and the separation distance for each

https://dx.doi.org/10.1021/acsami.0c20703
ACS Appl. Mater. Interfaces 2021, 13, 5133−5141

unit was about 2 mm. The working mechanism of the CEHF is schematically depicted in Figure 3d, also showing that the units were connected in parallel. This configuration allowed our CEHF to efficiently harvest mechanical energy from human footfalls and acted as a self-powered sensor. We measured the output current as a function of load resistances (Figure 3e), showing a peak power output of ∼5 mW at 1.5 MΩ. A longevity test of the CEHF was also carried out, which showed no obvious change in its output voltage for over 12,000 working cycles (Figure 3f), demonstrating good durability and stability.

The output performance of the CEHF under different working conditions was also investigated. Generally, people may walk, run, and jump on the floor, which corresponding to low, medium, and high driven frequency, respectively, for the CEHF. From the output voltage signals generated by different motion forms of an adult (Figure 4a), we could find that the output voltage generated by walking (∼200 V) was the smallest one of the three; however, it was still high enough for powering most of the electronic devices. Higher output also could be realized when the CEHF was driven by running (∼260 V) and jumping (∼360 V) due to their higher impulse force and driven frequency than those of walking. The different output peak profiles could be explained by the different initial working states of the CEHF. For walking and running, the initial state of the CEHF was in separation (Figure 3d II). It would come to the contacted state (Figure 3d I) when people stepped on. For jumping (vertical jumping), the initial state of the CEHF was in contact, and it would change to the separated state when people jumped up. The different working process led to the reversed output signals. Besides, driven force could also vary based on the person's body weight. When people with different weights walk on the CEHF, such as a child (∼20 kg), a teenager (∼40 kg), and an adult (∼60 kg), different driven forces will act on the CEHF generating output with different amplitudes (Figure 4b). The output voltage increased with the increasing of people's weight, which could be attributed to closer contact and increased friction of the triboelectric materials caused by the bigger force. Although the child had the lowest weight, an output voltage of ∼100 V could still be realized by our CEHF. In addition, the CEHF could be directly installed or integrated with regular flooring materials such as hardwood and carpet to meet more personalized design and application demands (Figure 4c). Carpet will absorb some of the mechanical energy, lowering the effective strain rate which resulted in a smaller average output than hardwood. Additionally, the CEHF was packaged by the polythene film to prevent water infiltration, which could limit the TENG in a practical application. To test this, 30 mL of water was poured on the CEHF and left undisturbed for 15 min before its output voltage was recorded to examine its waterproof ability. As shown in Figure 4d, the CEHF could work normally after being wetted by water, which showed its strong ability in resisting the influence of water.

To explore the wireless application of the CEHF, a real-time wireless transmission sensing system was designed and is schematically shown in Figure 5a. When an individual steps on the CEHF, the converted electric energy simultaneously sensed the foot steps and powered a RF transmission system. As such, useful foot traffic information could be collected remotely and be processed in real-time. The wireless transmitter system was specially designed to store the limited power generated by the CEHF. Figure 5b shows the schematic circuit diagram of the self-powered wireless transmitter sensing system which included the CEHF, storage circuit, wireless signal (433 MHz) generating circuit, and the receiver circuit. The receiver contained a LT DC1120A receiver board with a filter with cutoff frequencies at ∼400 and ∼470 MHz, an ST NUCLEO-F072RB microcontroller board, a green light-emitting diode (LED) that acted as a display/functional unit, and a 9 V power source. The detailed circuit diagram of each part is shown in Figures S1−S3. The AC output current of the CEHF generated by footsteps was converted into DC output by a rectifying circuit and stored in four 80 nF capacitors. As shown in Figure 5c, a maximum output current of just under 250 μA was achieved when a person with a weight of ∼60 kg stepped on top of it. A control circuit automatically discharged the stored energy once the 12 V threshold was reached, powering the wireless module that transmitted a wireless signal. This signal could be immediately received by the receiver box that was placed 0.25 m away from the transmitter. A lighted-up green LED indicated the signal reception, which is seen in Figure 5d, Videos S1, and S2. This function demonstrated the capability of power-free and wireless sensing by a person standing on the floor.

CONCLUSIONS

In this work, a high performance CEHF was successfully designed and fabricated via a scalable approach. This was achieved through the use of tribopositive weighing paper and tribonegative nitrocellulose paper, roughened weighing paper surface via a new mechanical exfoliation method, and a multilayered device structure. Our CEHF exhibited excellent output performance with a maximum output voltage, current, and power peak values of 360 V, 250 μA, and 5 mW, respectively. It could be directly installed or integrated with regular flooring products to effectively convert human body movements into electricity and showed good durability and stability even when wetted by water. Moreover, a wireless transmission sensor system with a 1:1 footstep-to-signal (transmitted and received) ratio was able to be instantaneously powered by the CEHF entirely based on cellulosic triboelectric materials. This work provides a feasible and effective way to utilize eco-friendly cellulose materials in constructing self-powered wireless transmission systems for future smart city.

EXPERIMENTAL SECTION

Fabrication of Devices. Four commercial paper products: weighing paper (Fisher Scientific, thickness of ∼50 μm), printer paper (Hammermill, thickness of ∼100 μm), tissue paper (Kimberly-Clark Professional, thickness of ∼100 μm), and crafting paper (thickness of ∼100 μm) were used to pair with nitrocellulose paper with a size of 2 cm× 2 cm, assembling four TENGs with commonly used contact-separation working mode. To keep the same thickness of tribopositive paper materials, two pieces of weighing paper was stacked together as one frictional layer in the experiment. In the fabrication process, copper tape (thickness of 50 μm) was first attached on a flat wood substrate as one electrode, and paper which acted as a tribopositive frictional layer was closely attached on the electrode. Then, nitrocellulose paper with a copper electrode on the back was fixed on a controlled oscillating bar (LinMot E1100) as the tribonegative frictional layer. By changing the paper placed on the wooden substrate, the outputs of the four TENGs which shared the same nitrocellulose paper frictional layer could be characterized.

For the fabrication of the CEHF, the multilayered structure was composed of four thin wood substrates, six frictional layers (three nitrocellulose paper layers and three weighing paper layers), and three foam spacers (thickness of each one is ∼3 mm). Double-sided tape

https://dx.doi.org/10.1021/acsami.0c20703
ACS Appl. Mater. Interfaces 2021, 13, 5133−5141

(Scotch, thickness of 100 μm) was used to fix the frictional layer and spacer on the substrates. From the bottom to top, nitrocellulose paper with copper tape was attached on the upper surface of the first substrate (thickness of ∼0.8 mm) with reserved edge (width of ∼1 cm) unfilled for subsequently fixing foam spacers. Then, two weighing paper frictional layers with copper tape were attached on the upper and lower surfaces of the second substrate (thickness of ∼1.7 mm) also with reserved edges unfilled. The edge on the lower surface was connected to the spacer on the first substrate, and the edge on the upper surface was used to fix another foam spacer. The fabrication of third (thickness of ∼1.7 mm) and fourth (thickness of ∼0.8 mm) substrates was basically the same as the second and first, respectively, with the exception of having the opposite frictional layer to their respective counterparts. The Cu tapes attached on nitrocellulose paper and weighing paper were connected together through Cu wire, forming two electrodes for electrical measurement. Finally, the assembled structure was packaged by a polythene film (Stretch-Tite, thickness of ∼20 μm) with over-provisioning space to resist the influence of water, and two thick wood substrates (thickness of ∼3 mm) were fixed on the top and bottom surfaces of the packaged structure protecting it from mechanical damage.

Integration of the CEHF and Commercial Flooring Materials. The two commercial flooring materials, hardwood and carpet, were first cut into small pieces as big as the CEHF panel, and then they were attached on the top surface of the CEHF by epoxy resin adhesive. The whole device can be used for electrical measurement after curing for 30 min at room temperature.

Electric Characterizations. TENGs with an area of 2 cm × 2 cm were driven by a computer-controlled actuator (LinMot E1100) with amplitude, frequency, and force of 1 cm, 1.1 Hz, and 6 N. The CEHF was driven by the LinMot in the output power and longevity tests with amplitude, frequency, and force of 1 cm, 1.1 Hz, and 20 N. For the rest of the measurements, the CEHF was driven by human steps. The voltage outputs of all devices were measured by a multimeter (DMM 6500, Keithley, internal resistance 10 MΩ). The short-circuit currents of all devices were measured by a low-noise current preamplifier (SR570, Stanford). The output charge density was measured by an electrometer (6514, Keithley) with the nitrocellulose as a tribonegative material.

■ ASSOCIATED CONTENT

Supporting Information

The Supporting Information is available free of charge at https://pubs.acs.org/doi/10.1021/acsami.0c20703.

Detailed circuit diagram of the wireless transmission sensing system and detailed circuit diagram of the transmitter, receiver, and micro controller unit (PDF)

Instantaneous powering of a wireless transmission sensor system by the CEHF (AVI)

Instantaneous powering of a wireless transmission sensing system after wetting with water (AVI)

■ AUTHOR INFORMATION

Corresponding Author

Xudong Wang − *Department of Materials Science and Engineering, University of Wisconsin-Madison, Madison, Wisconsin 53706, United States;* orcid.org/0000-0002-9762-6792; Email: xudong.wang@wisc.edu

Authors

Long Gu − *Department of Materials Science and Engineering, University of Wisconsin-Madison, Madison, Wisconsin 53706, United States;* orcid.org/0000-0001-7879-6086

Lazarus German − *Department of Materials Science and Engineering, University of Wisconsin-Madison, Madison, Wisconsin 53706, United States*

Tong Li − *Department of Materials Science and Engineering, University of Wisconsin-Madison, Madison, Wisconsin 53706, United States*

Jun Li − *Department of Materials Science and Engineering, University of Wisconsin-Madison, Madison, Wisconsin 53706, United States;* orcid.org/0000-0002-7498-6736

Yan Shao − *Department of Materials Science and Engineering, University of Wisconsin-Madison, Madison, Wisconsin 53706, United States*

Yin Long − *Department of Materials Science and Engineering, University of Wisconsin-Madison, Madison, Wisconsin 53706, United States;* orcid.org/0000-0002-6602-0210

Jingyu Wang − *Department of Materials Science and Engineering, University of Wisconsin-Madison, Madison, Wisconsin 53706, United States*

Complete contact information is available at: https://pubs.acs.org/10.1021/acsami.0c20703

Author Contributions

§Long Gu and Lazarus German with equal contribution.

Notes

The authors declare the following competing financial interest(s): Lazarus German and Xudong Wang are co-founders of and own stock in EWPanel, LLC. All other authors declare no conflict of interest.

■ ACKNOWLEDGMENTS

The authors acknowledge the National Science Foundation Award # IIP-STTR Phase I 1843965.

■ REFERENCES

(1) Plageras, A. P.; Psannis, K. E.; Stergiou, C.; Wang, H.; Gupta, B. B. Efficient IoT-Based Sensor BIG Data Collection-Processing and Analysis in Smart Buildings. *Future Generat. Comput. Syst.* **2018**, *82*, 349−357.

(2) Tu, J.; Torrente-Rodríguez, R. M.; Wang, M.; Gao, W. The Era of Digital Health: A Review of Portable and Wearable Affinity Biosensors. *Adv. Funct. Mater.* **2020**, *30*, 1906713.

(3) Risteska Stojkoska, B. L.; Trivodaliev, K. V. A Review of Internet of Things for Smart Home: Challenges and Solutions. *J. Cleaner Prod.* **2017**, *140*, 1454−1464.

(4) Wu, Z.; Cheng, T.; Wang, Z. L. Self-Powered Sensors and Systems Based on Nanogenerators. *Sensors* **2020**, *20*, 2925.

(5) Niu, S.; Matsuhisa, N.; Beker, L.; Li, J.; Wang, S.; Wang, J.; Jiang, Y.; Yan, X.; Yun, Y.; Burnett, W.; Poon, A. S. Y.; Tok, J. B.-H.; Chen, X.; Bao, Z. A Wireless Body Area Sensor Network Based on Stretchable Passive Tags. *Nat. Electron.* **2019**, *2*, 361−368.

(6) Tian, X.; Lee, P. M.; Tan, Y. J.; Wu, T. L. Y.; Yao, H.; Zhang, M.; Li, Z.; Ng, K. A.; Tee, B. C. K.; Ho, J. S. Wireless Body Sensor Networks Based on Metamaterial Textiles. *Nat. Electron.* **2019**, *2*, 243−251.

(7) Li, T.; Feng, Z.-Q.; Qu, M.; Yan, K.; Yuan, T.; Gao, B.; Wang, T.; Dong, W.; Zheng, J. Core/Shell Piezoelectric Nanofibers with Spatial Self-Orientated β-Phase Nanocrystals for Real-Time Micro-pressure Monitoring of Cardiovascular Walls. *ACS Nano* **2019**, *13*, 10062−10073.

(8) Gu, L.; Liu, J.; Cui, N.; Xu, Q.; Du, T.; Zhang, L.; Wang, Z.; Long, C.; Qin, Y. Enhancing the Current Density of a Piezoelectric Nanogenerator Using a Three-Dimensional Intercalation Electrode. *Nat. Commun.* **2020**, *11*, 1030.

(9) Li, J.; Long, Y.; Yang, F.; Wei, H.; Zhang, Z.; Wang, Y.; Wang, J.; Li, C.; Carlos, C.; Dong, Y.; Wu, Y.; Cai, W.; Wang, X. Multifunctional Artificial Artery from Direct 3D Printing with Built-In Ferroelectricity and Tissue-Matching Modulus for Real-Time

Sensing and Occlusion Monitoring. *Adv. Funct. Mater.* **2020**, *30*, 2002868.
(10) Ryu, H.; Yoon, H. J.; Kim, S. W. Hybrid Energy Harvesters: Toward Sustainable Energy Harvesting. *Adv. Mater.* **2019**, *31*, 1802898.
(11) Vats, G.; Kumar, A.; Ortega, N.; Bowen, C. R.; Katiyar, R. S. Giant Pyroelectric Energy Harvesting and A Negative Electrocaloric Effect in Multilayered Nanostructures. *Energy Environ. Sci.* **2016**, *9*, 1335−1345.
(12) Costa, P.; Nunes-Pereira, J.; Pereira, N.; Castro, N.; Gonçalves, S.; Lanceros-Mendez, S. Recent Progress on Piezoelectric, Pyroelectric, and Magnetoelectric Polymer-Based Energy-Harvesting Devices. *Energy Technol.* **2019**, *7*, 1800852.
(13) Liu, J.; Gu, L.; Cui, N.; Xu, Q.; Qin, Y.; Yang, R. Fabric-Based Triboelectric Nanogenerators. *Research* **2019**, *2019*, 1091632.
(14) Cui, N.; Dai, C.; Liu, J.; Gu, L.; Ge, R.; Du, T.; Wang, Z.; Qin, Y. Increasing the Output Charge Quantity of Triboelectric Nanogenerators via Frequency Multiplication with a Multigap-Structured Friction Layer. *Energy Environ. Sci.* **2020**, *13*, 2069−2076.
(15) Liu, W.; Wang, Z.; Wang, G.; Liu, G.; Chen, J.; Pu, X.; Xi, Y.; Wang, X.; Guo, H.; Hu, C.; Wang, Z. L. Integrated Charge Excitation Triboelectric Nanogenerator. *Nat. Commun.* **2019**, *10*, 1426.
(16) Liu, J.; Gu, L.; Cui, N.; Bai, S.; Liu, S.; Xu, Q.; Qin, Y.; Yang, R.; Zhou, F. Core-Shell Fiber-Based 2D Woven Triboelectric Nanogenerator for Effective Motion Energy Harvesting. *Nanoscale Res. Lett.* **2019**, *14*, 311.
(17) Xu, W.; Zheng, H.; Liu, Y.; Zhou, X.; Zhang, C.; Song, Y.; Deng, X.; Leung, M.; Yang, Z.; Xu, R. X.; Wang, Z. L.; Zeng, X. C.; Wang, Z. A Droplet-Based Electricity Generator with High Instantaneous Power Density. *Nature* **2020**, *578*, 392−396.
(18) Long, Y.; Wei, H.; Li, J.; Yao, G.; Yu, B.; Ni, D.; Gibson, A. L.; Lan, X.; Jiang, Y.; Cai, W.; Wang, X. Effective Wound Healing Enabled by Discrete Alternative Electric Fields from Wearable Nanogenerators. *ACS Nano* **2018**, *12*, 12533−12540.
(19) Li, J.; Kang, L.; Long, Y.; Wei, H.; Yu, Y.; Wang, Y.; Ferreira, C. A.; Yao, G.; Zhang, Z.; Carlos, C.; German, L.; Lan, X.; Cai, W.; Wang, X. Implanted Battery-Free Direct-Current Micro-Power Supply from in Vivo Breath Energy Harvesting. *ACS Appl. Mater. Interfaces* **2018**, *10*, 42030−42038.
(20) Wu, C.; Wang, A. C.; Ding, W.; Guo, H.; Wang, Z. L. Triboelectric Nanogenerator: A Foundation of the Energy for the New Era. *Adv. Energy Mater.* **2019**, *9*, 1802906.
(21) Jiang, C.; Wu, C.; Li, X.; Yao, Y.; Lan, L.; Zhao, F.; Ye, Z.; Ying, Y.; Ping, J. All-Electrospun Flexible Triboelectric Nanogenerator Based on Metallic MXene Nanosheets. *Nano Energy* **2019**, *59*, 268−276.
(22) Wang, N.; Wang, X.-X.; Yan, K.; Song, W.; Fan, Z.; Yu, M.; Long, Y.-Z. Anisotropic Triboelectric Nanogenerator Based on Ordered Electrospinning. *ACS Appl. Mater. Interfaces* **2020**, *12*, 46205−46211.
(23) Cheng, X.; Miao, L.; Su, Z.; Chen, H.; Song, Y.; Chen, X.; Zhang, H. Controlled Fabrication of Nanoscale Wrinkle Structure by Fluorocarbon Plasma for Highly Transparent Triboelectric Nanogenerator. *Microsyst. Nanoeng.* **2017**, *3*, 16074.
(24) Zhang, Y.; Wu, M.; Zhu, Q.; Wang, F.; Su, H.; Li, H.; Diao, C.; Zheng, H.; Wu, Y.; Wang, Z. L. Performance Enhancement of Flexible Piezoelectric Nanogenerator via Doping and Rational 3D Structure Design For Self-Powered Mechanosensational System. *Adv. Funct. Mater.* **2019**, *29*, 1904259.
(25) Shang, W.; Gu, G. Q.; Yang, F.; Zhao, L.; Cheng, G.; Du, Z.-l.; Wang, Z. L. A Sliding-Mode Triboelectric Nanogenerator with Chemical Group Grated Structure by Shadow Mask Reactive Ion Etching. *ACS Nano* **2017**, *11*, 8796−8803.
(26) Wang, X.; Yao, C.; Wang, F.; Li, Z. Cellulose-Based Nanomaterials for Energy Applications. *Small* **2017**, *13*, 1702240.
(27) Yao, C.; Yin, X.; Yu, Y.; Cai, Z.; Wang, X. Chemically Functionalized Natural Cellulose Materials for Effective Triboelectric Nanogenerator Development. *Adv. Funct. Mater.* **2017**, *27*, 1700794.
(28) Chen, S.; Jiang, J.; Xu, F.; Gong, S. Crepe Cellulose Paper and Nitrocellulose Membrane-Based Triboelectric Nanogenerators for Energy Harvesting and Self-Powered Human-Machine Interaction. *Nano Energy* **2019**, *61*, 69−77.
(29) Chen, S.; Song, Y.; Ding, D.; Ling, Z.; Xu, F. Flexible and Anisotropic Strain Sensor Based on Carbonized Crepe Paper with Aligned Cellulose Fibers. *Adv. Funct. Mater.* **2018**, *28*, 1802547.
(30) Nie, S.; Guo, H.; Lu, Y.; Zhuo, J.; Mo, J.; Wang, Z. L. Superhydrophobic Cellulose Paper-Based Triboelectric Nanogenerator for Water Drop Energy Harvesting. *Adv. Mater. Technol.* **2020**, *5*, 2000454.
(31) Wu, C.; Kima, T. W.; Sung, S.; Park, J. H.; Li, F. Ultrasoft and Cuttable Paper-Based Triboelectric Nanogenerators for Mechanical Energy Harvesting. *Nano Energy* **2018**, *44*, 279−287.
(32) Wang, J.; Deng, Y.; Qian, Y.; Qiu, X.; Ren, Y.; Yang, D. Reduction of Lignin Color via One-Step UV Irradiation. *Green Chem.* **2016**, *18*, 695−699.
(33) Shi, K.; Zou, H.; Sun, B.; Jiang, P.; He, J.; Huang, X. Dielectric Modulated Cellulose Paper/PDMS-Based Triboelectric Nanogenerators for Wireless Transmission and Electropolymerization Applications. *Adv. Funct. Mater.* **2020**, *30*, 1904536.

https://dx.doi.org/10.1021/acsami.0c20703
ACS Appl. Mater. Interfaces 2021, 13, 5133−5141